

**Title:**

Investigation of Ta-MX/Z-Phase and Laves Phase as Precipitation Hardening Particles in a 12 Pct Cr Heat-Resistant Steel

**Authors:**

J. P. Sanhueza, D. Rojas, O. Prat, J. García, M. F. Meléndrez, S. Suarez

This is a post-peer-review, pre-copyedit version of an article published in *Metallurgical and Materials Transactions A*

The final authenticated version is available online at: <https://doi.org/10.1007/s11661-018-4654-8>

**Cite as:**

Sanhueza, J.P., Rojas, D., Prat, O. et al. Metall and Mat Trans A (2018) 49: 2951. <https://doi.org/10.1007/s11661-018-4654-8>



**Title**

Investigation of Ta-MX/Z-phase and Laves Phase as precipitation hardening particles in a 12%Cr heat resistant steel

**Author**

J. P. Sanhueza<sup>a</sup>, D. Rojas<sup>a,\*</sup>, O. Prat<sup>a</sup>, J. Garcia<sup>b</sup>, M.F. Melendrez<sup>a</sup>, S. Suarez<sup>c</sup>

**Affiliation Address**

a. Universidad de Concepción, Departamento de Ingeniería de Materiales, Edmundo Larenas 270, Concepción, Chile

b. AB SandvikCoromant R&D, Lerkrogsvägen 19, Stockholm, SE 126 80, Sweden.

c. Department of Materials Science, Saarland University, 66123 Saarbrücken, Germany

**\*Corresponding Author:**

David Rojas: davrojas@udec.cl

## **Abstract**

A 12%Cr martensitic/ferritic steel was designed and produced to study Laves and Z-phase as precipitation hardening particles under creep conditions at 650°C. To ensure the precipitation of Laves after tempering, additions of W and Cu were selected according to thermodynamic calculations. It is known that Z-phase formation does not follow the classical nucleation theory. Indeed, MX particles are transformed into Z-phase by Cr diffusion from the matrix to the precipitate. Therefore, to promote fast Z-phase formation, Ta, Co and N additions were used to produce Ta-MX which will be transformed into Z-phase. As main results, Laves precipitation was successfully achieved after tempering with a particle size of 196nm. Concerning Z-phase, the transformation of Ta-MX into Z-phase after tempering was confirmed by the formation of hybrid nanoparticles of 30nm. Although, W and Ta have a low diffusion in martensitic/ferritic matrix, characterization of the precipitates after isothermal aging revealed that Laves and Z-phase have a fast growth kinetic, reaching 400nm and 143nm respectively at 8760h. As consequence, creep test at 650°C showed premature fails after few thousand hours. Therefore, investigations focused on the growth and coarsening behavior of Laves and Z-phase, seem to be the next researcher field of martensitic/ferritic steels.

**Keywords:** TEM characterization, 12%Cr steels, Z-Phase, Laves Phase, Creep, Thermo-  
Calc Modelling

## 1. Introduction

Martensitic/ferritic creep resistant steels are a widely used in the new supercritical power plants (600°C/30 MPa) for key components material such as: steam pipes, turbines and boilers. They combine high creep strength, oxidation resistance, good weldability, thermal fatigue resistance and competitive production costs [1, 2]. Nowadays, grade T/P91 and T/P92 are the most common martensitic/ferritic steels used in fossil fuel power plants due to their high microstructural stability [3, 4]. In general, precipitation hardening considering  $M_{23}C_6$  carbides and MX particles is the main creep strengthening mechanism in 9-12%Cr heat resistant steel [5, 6]. A high volume fraction of  $M_{23}C_6$  carbides nucleate heterogeneously on sub-boundaries and grain boundaries avoiding the recovery of the martensitic/ferritic matrix during long-term creep [7, 8]. Furthermore, additional creep strength is obtained by precipitation of MX carbonitrides along sub-grain boundaries as in T/P91 steels, which have a creep rupture strength of 94 MPa at 600°C/10<sup>5</sup>h [9, 10]. Also, an increment of 20% on rupture strength can be obtained by the addition of W and B, as has been demonstrated in T/P92 steels [7, 11]. Moreover, W and B increase the creep strength by solid solution hardening and reduce the coarsening rate of  $M_{23}C_6$  carbides, respectively, avoiding the recovery of the martensitic/ferritic matrix [12, 13]. Nowadays, new environmental regulations in regards of CO<sub>2</sub> emissions have motivated many researching groups to focus their efforts in the development of new 9-12%Cr creep resistant steels under operating condition of 650°C/30MPa, which would lead to a higher efficiency of the steam cycle, therefore decreasing CO<sub>2</sub> emissions of fossil fuel power plants [14, 15]. Consequently, first researches on conventional 9%Cr steel (T/P91 and T/P92) showed that oxidation resistance of these materials are not enough to operate at 650°C [1, 16]. Thus, increasing Cr content to 12% was the first attempt to overcome this barrier, unfortunately

with no successful results. Although, superior oxidation resistance was obtained, the long-term creep resistance declined drastically due to the transformation of MX particles into detrimental coarse Z phase [17]. The MX particles are carbides, nitrides and/or carbonitrides depending on the chemical composition of the alloy, where M denotes a metallic element such as V, Nb and/or Ta and X denotes C and/or N [11, 18]. However, the MX precipitates are a metastable phase in martensitic/ferritic steels and during service, under certain temperature and time they will be transformed into Z phase, a thermodynamically stable nitride [19, 20]. Time for fully transformation of MX carbonitrides into Z phase can last months, years or decades, depending on the chemical composition of the alloy [21, 22]. Also, due to the beneficial effect of W in solid solution on the ferritic crystal lattice of T/P92 steels, investigation on its effect at higher concentration for the long-term creep was carried out. Researchers found that although W is beneficial to short-term creep, under long-term creep Laves phase ( $\text{Fe}_2\text{W}$ ) precipitates heterogeneously at grain and laths boundaries resulting in solid solution strengthening loss [23, 24]. Currently, the investigations on Z and Laves phase precipitation kinetics have become a very important research field, which has had significant advances aiming to obtain Z phase particles after heat treatment, before service time [21]. Therefore, as design concept, Z and Laves phases could be used as reinforcement particles to promote precipitation hardening, with small particle size and even distribution throughout the matrix, to enhance the creep resistance [25, 26]. The main objective of this paper is to investigate a 12%Cr steel designed to have a high precipitation rate and driving force for Z and Laves phase formation, respectively [27, 28]. Thermodynamic modeling, creep test and characterization of precipitates after isothermal aging at 650°C were carried out.

## 2. Experimental procedure

### 2.1 Thermodynamic modeling

Thermo-Calc software package based on the CALPHAD method has been successfully employed for alloy design considering multicomponent and multiphase systems [21, 28]. The core of this method is the calculation of the Gibbs energy of a phase as a function of both its composition temperature and pressure. Within this approach, the problem of predicting equilibrium and evaluation of phase stability is essentially mathematical, although far from simple due to the number of variables involved in the minimization process [19]. The software is linked to various databases and interfaces, where all thermodynamic information is stored as Gibbs energy. Upon modeling, time and costs of trial-and-error for conventional alloy development can be reduced. All calculations were carried out based on Thermo-Calc database TCFE8 [13,29].

### 2.2 Alloy production

The alloy studied was produced by vacuum induction melting. Its chemical composition is shown in Table 1. The sample was hot forged at 1150°C with an area reduction of 70% and subsequently air-cooled. Heat treatment considers an austenization at 1070°C for 0.5 h and air-cooling, followed by 780°C/2h tempering.

### 2.3 Creep tests and isothermal aging

Tensile creep tests in air at 650°C ( $\pm 5$ K) with constant load between 80 and 250MPa were used to determine the creep rupture times. Standard cylindrical samples according to DIN50125 B 4 $\times$ 20 were used. Additionally, samples of 1x1x1 cm were isothermally aged at 650°C for 1440 h and 8760 h to investigate the evolution of precipitates.

## 2.4 Characterization

Transmission Electron Microscopy (TEM) and High Resolution Transmission Electron Microscopy (HRTEM) were used in order to characterize the microstructure of the alloy. A Jeol JEM-2010F (TEM) and JEM-2100 (HRTEM) microscopes equipped with Energy Dispersive Spectroscopy (EDS) analyzer were used. In order to avoid the effect of the martensitic/ferritic matrix during the characterization, conventional bulk carbon replication was used [9, 30]. The main purpose of carbon replica is to remove the magnetic effect of matrix and to prevent overlaps of EDS and diffraction pattern between precipitates and matrix [25, 31].

Chemical composition, crystalline structure and particle size of precipitates were measured by qualitative EDS analysis. Diffraction pattern and Feret's diameter, were indexed using an image software editor. Furthermore, to ensure a good reliability of measurements, more than 100 particles per each precipitates were analyzed (average chemical composition and particle size) [1].

The d-spacing obtained by diffraction pattern was compared to values found in literature. Three types of crystalline structures were studied, face centered cubic, hexagonal closed packing and tetragonal. More information on the relation between d-spacing of each crystalline structure with its lattice parameter, refer to references [32, 33]. Table 2 shows the lattice parameters considered for TaC carbide, Ta(C,N) carbonitride, TaN nitride, Z and Laves phase [26, 34]. In the case of Z-phase, lattices parameters "a" and "c" calculated by Danielsen and Hald, and Ettmayer were considered [34, 35]. In some cases particles with the chemical composition of Z phase can be indexed as tetragonal with a lattice parameter of  $a=0.296$  nm and  $c=0.739$  nm (Danielsen and Hald) and in other cases particles can be indexed considering the lattice parameters  $a=0.425$  nm and  $c=0.733$  nm (Ettmayer).

In order to index a single crystal diffraction pattern, the angle  $\theta$  between two planes,  $(h_1k_1l_1)$  and  $(h_2k_2l_2)$  in a crystal system must be calculated. As an example for a tetragonal system, the following equation can be used [32]:

$$\text{Tetragonal system} \quad \cos \theta = \frac{\frac{(h_1h_2+k_1k_2)}{a^2} + \frac{l_1l_2}{c^2}}{\sqrt{\left\{\left(\frac{h_1^2+k_1^2}{a^2} + \frac{l_1^2}{c^2}\right)\left(\frac{h_2^2+k_2^2}{a^2} + \frac{l_2^2}{c^2}\right)\right\}}} \quad (1)$$

Depending on the crystalline structure and once the most probable diffracted planes are identified, calculation of the angles between them and the comparison to formula (1) are necessary. The difference between experimental measurements of the angle formed by two planes in the diffraction pattern and angle  $\theta$  (theoretical) cannot exceed 1 degree.

### 3. Results and discussion

#### 3.1 Alloy design

12%Cr heat resistant steel with tailor-made microstructure was designed and produced in order to obtain Z and Laves phase as stable precipitates at 650°C. To achieve this, elements that increase the stability and driving force for the formation of Laves and Z phase were added [27, 28]. It is widely known that in 9-12%Cr heat resistant steel precipitation of Laves phase occurs during service with a low nucleation rate and a higher mobility of the interface Particle/Matrix. Furthermore, the precipitation process usually starts after hundred or thousand hours under service condition depending on the chemical composition as well as on temperature. As an example, in T/P91 steel, precipitation of Fe<sub>2</sub>Mo-Laves phase was observed around 10.000h at 550°C while in T/P92 steel Fe<sub>2</sub>(W, Mo) particles were found



after 2.000h at 650°C [5, 23]. In general, there are disagreements on the effect of Mo and W in creep strength of 9-12%Cr steels [28, 36]. On one hand, researchers found that despite W and Mo are beneficial to short term creep, under long term creep these elements segregate at micro-grain boundaries promoting the heterogeneous precipitation of Laves phase, thus losing the solid solution strengthening [3, 37]. On the other hand, the excellent long-term stability of the W-alloyed 9Cr steel (T/P92) seems to contradict this finding. Experimental evidence shows and quantifies that solid solution strengthening mechanism is sparse [2]. In the design of creep resistant materials, size, dispersion, thermodynamic stability, growth rate and coarsening rate of phases determine its contribution to creep resistance [11, 13]. Size and dispersion of phases can be controlled by the nucleation rate, and if a small particle size distribution is obtained together with a low inter-particle distance, an increase in the Orowan stress can be achieved [10, 38]. Equation (2) describes the steady state nucleation rate ( $J_s$ ), where  $Z$  denotes the Zeldovich factor,  $\beta^*$  is the rate at which atoms are attached to the critical nucleus,  $N_0$  is the number of available nucleation sites per unit volume,  $\Delta G_m^{\alpha \rightarrow \beta}$  refers to the maximum driving force for the  $\alpha \rightarrow \beta$  phase transformation,  $\sigma$  is the interfacial energy of the  $\beta$  precipitates,  $V_m^\beta$  is the molar volume of the  $\beta$  phase,  $k$  is the Boltzmann's constant, and  $T$  means the absolute temperature [4, 21]:

$$J_s = Z\beta^*N_0\exp\left(-\frac{16\pi\sigma^3}{3(\Delta G_m^{\alpha \rightarrow \beta}/V_m^\beta)^2 kT}\right) \quad (2)$$

To increase the nucleation rate of Laves phase, the focus was to increase the driving force ( $\Delta G_m^{\alpha \rightarrow Laves}$ ) and the number of available nucleation sites per unit volume ( $N_0$ ) by the addition of W and Cu, respectively. The addition of W increases the stability of Laves phase at high temperature and Cu promotes the precipitation of Cu-rich particles which act as nucleation sites for Laves phase [28, 39]. Thermodynamic information as phase equilibrium diagram and the maximum driving force for Laves phase nucleation were obtained in Thermo-Calc. The maximum driving force can be obtained by finding the parallel tangent lines or surfaces passing through the alloy composition of the matrix. This is a routine calculation in Thermo-Calc [1, 38]. Figure 1A shows the calculation carried out in Thermo-Calc for the driving force of Laves phase in 12CrWTaCo, T/P91 and T/P92 steels. Figure 1B shows the effect of adding W or Mo to the driving force of Laves phase in the designed alloy. Analyzing Fig. 1A it is clear that alloy 12CrWTaCo was designed to have a nucleation rate of Laves Phase faster than conventional 9-12%Cr steels at tempering temperature (780°C). Also, a higher driving force for Laves Phase can be achieved by adding W instead of Mo (see Fig. 1B). The thermodynamic modeling predicts that Laves phase stability can be increased to temperatures about 1000°C by adding 3.8% W and 1.0% Cu.

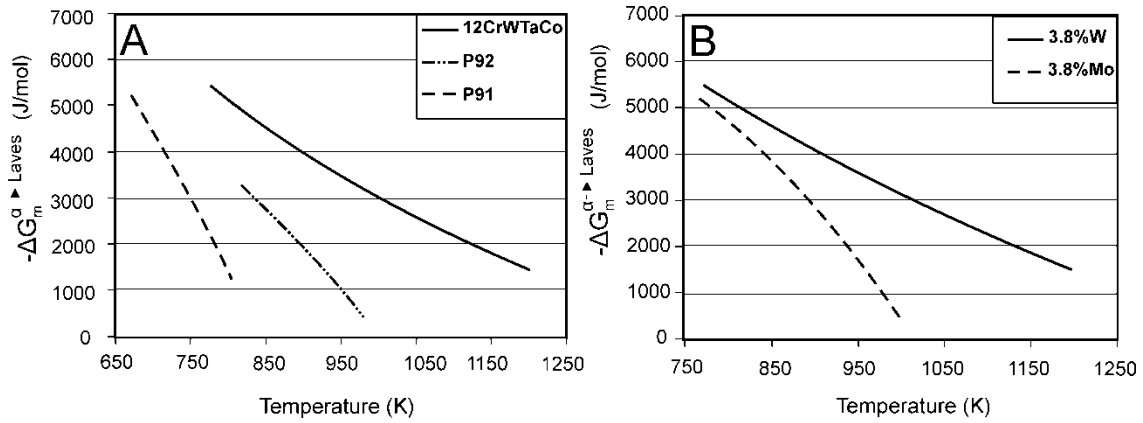


Fig. 1 Maximum driving force variation for the  $F \rightarrow Laves$  phase transformation versus temperature (Kelvin). A) Driving force of Laves phase calculated for 12CrWTaCo, P91 and P92. B) Effect of W and Mo in the driving force of Laves phase for the designed alloy.

The precipitation of Z phase was not focused on increasing the nucleation rate, since its formation does not follow the classical nucleation theory. Indeed, the formation of Z phase is a diffusion controlled transformation following the sequence described below: i) movement of Cr atoms from matrix to  $\alpha$ -Ferrite/MX interface, ii) flux of Cr atoms across the interface, and iii) formation of an alternating structure of Cr-rich and Ta-rich layers inside the MX particle by the diffusion of Cr atoms [26, 27]. This process changes the FCC crystalline structure (NaCl-type) of MX precipitates to a tetragonal Z phase structure [25]. In general, in 9-12%Cr steels there are three types of Z phase precipitates: CrVN, CrNbN and CrTa<sub>2</sub>N, each one with a different precipitation rate. The CrTa<sub>2</sub>N nitride has the fastest kinetics of precipitation and CrVN the slowest one [35]. Hence, 0.8%Ta was added in order to obtain faster precipitation kinetics of the CrTa<sub>2</sub>N-Z phase in the designed alloy. Furthermore, the addition of 4.2%Co was considered in order to stabilize an austenitic phase field at high temperature, thus the martensitic transformation may take place

avoiding the formation of delta ferrite during solidification [1, 13]. Additionally, it has been reported that Co addition accelerate the transformation of MX particles into Z phase [40, 41]. They have suggested that Co rises the Cr activity in the matrix, promoting the Z phase formation. Figure 2 shows the phase diagram obtained in Thermo-Calc for the alloy 12CrWTaCo. It can be seen that Ferrite, Laves phase, Ta-MX,  $M_{23}C_6$  and Cu-rich particles are the main stable phases at tempering (780°C) and service (650°C) temperature [18, 26]. However, this should not be understood as the Z phase not being thermodynamically stable for the alloy; in TCFE8 database, CrTa<sub>2</sub>N-Z phase is not yet defined [29].

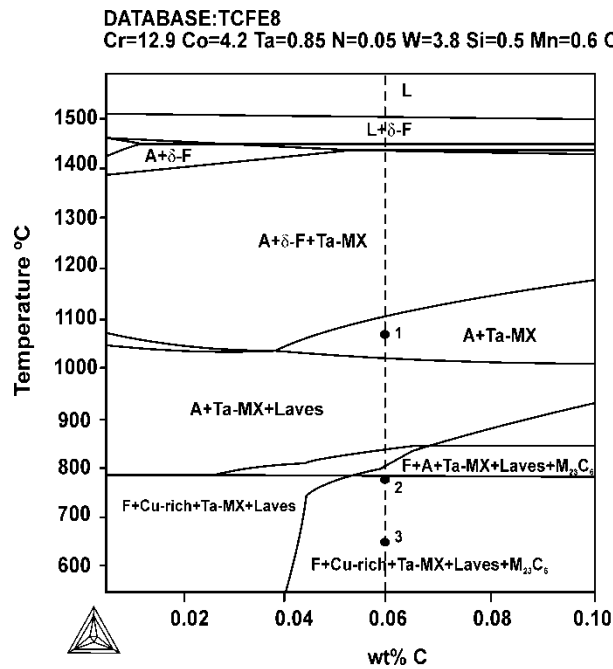


Fig. 2 Thermo-Calc phase diagrams of the investigated alloy 12CrWTaCo (F=ferrite, A=austenite). Heat treatments and creep test temperature were included (1=Austenization temperature, 2=Tempering temperature, 3=Creep test and isothermal annealing temperature).

Additionally, thermodynamic calculations were carried out in order to obtain the equilibrium composition of phases at the heat treatments and creep test temperature. the chemical composition of phases at the austenization temperature (1070°C) are shown in table 3 were attached. It is clear that equilibrium phases at this temperature are Austenite and Ta-MX particles. On the other hand, table 4 shows the chemical composition of equilibrium phases at tempering temperature (780°C). Similar results are shown in table 5; however thermodynamic calculations were carried out at the creep test temperature (650°C).

### *3.2 Characterization of precipitates after heat treatment (780°C/2h)*

In order to check the accuracy of the Thermo-Calc software in comparison to the prediction of the equilibrium phases, identification of precipitates after tempering at 780°C/2h were carried out. The analysis on extraction replica shows that only Laves phase and Ta-MX are present after tempering. Both phases were identified by EDS and diffraction pattern. It is expected that Cu-rich particles are together with Laves phase particles; as a result an extra pick from the Cu should appear in the EDS pattern of the Laves phase. However, the identification was not possible due to the energies associated to the electronic transitions of Cu atoms in the particle overlapping with those of the copper grid. On the other hand,  $M_{23}C_6$  carbides were not found in the microstructure, suggesting that this phase is not thermodynamically stable. In fact, metallic atoms composition of  $M_{23}C_6$  carbides (79Cr-14Fe-5W-2Mn-0.02Co) calculated from table 5 does not match with any of the analyzed particles in table 6. This can be explained by the higher affinity of C for Ta compared to Cr and the high content of Ta in the alloy. Consequently, Ta-MX particles consume all the available carbon during their precipitation process [42]. It is probably that for higher carbon

content,  $M_{23}C_6$  carbides can be thermodynamically stabilized in the alloy. Furthermore, in case there is no formation of  $M_{23}C_6$  carbides [13], an increase in the available nucleation sites of Laves phase can be expected. Figure 3 shows an image taken from an extracted replica sample of the alloy 12CrWTaCo which still keeps the distribution of precipitates along prior austenite grain boundary, lath boundary and inside the grain. From this image it can be seen the different nucleation sites of particles depending of its precipitation kinetics.

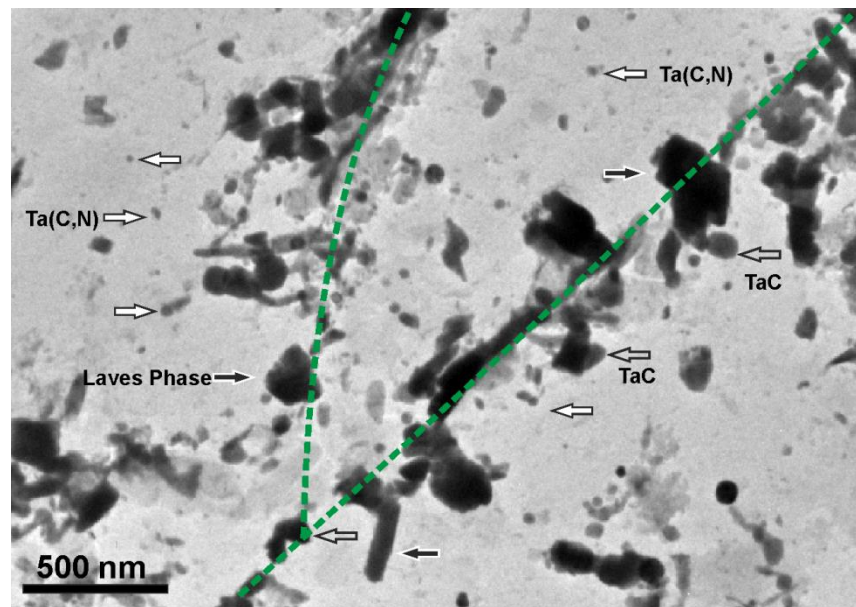


Fig. 3 TEM image of an extracted replica of the alloy after tempering (780°C/2h). Ta(C, N) carbonitrides (white arrows), TaC carbides (gray arrows) and Laves phase (black arrows). The green dotted line represents a prior austenite grain boundary and a lath boundary.

The characterization of Laves phase is shown in fig. 4, EDS analysis identified that forming elements are Fe, Cr and W. Also, the atomic composition of Laves phase was measured and incorporated in table 7. As it can see results are in good agreement with the predicted composition by ThermoCalc. Moreover, indexation of diffraction pattern (Fig. 4 B)

confirms the typical hexagonal crystal structure of this phase and the presence of stacking faults can also be appreciated [35]. As shown in Table 7 a relatively small particle size of Laves phase was reached after tempering (196 nm). This combined with a high volume fraction of the Laves phase is suitable to generate a pinning force for dislocation glide and interfaces migration.

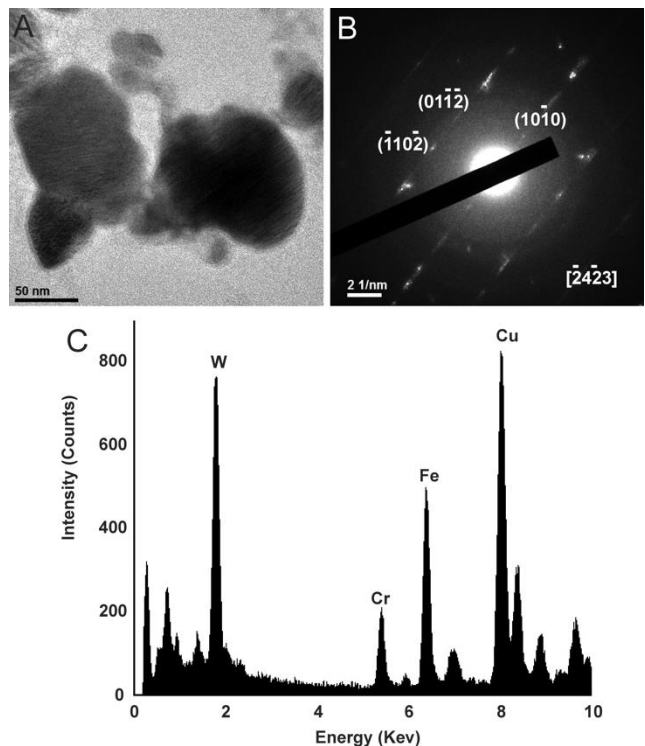


Fig. 4 TEM image of an extracted replica of the alloy after tempering (780°C/2h). A) Image of Laves phase. B) Diffraction pattern of Laves phase. C) EDS analysis of Laves phase.

Two types of Ta-MX particles were identified depending on the nucleation sites and its average size (see fig. 3) [13]. First, TaC carbides were found along prior austenite grain boundaries and block boundaries with a mean particle size of 196 nm, these particles were formed during solidification which did not dissolve during austenization heat treatment [43,

44]. On the other hand, Ta(C, N) carbonitrides (30 nm) were observed along sub-grain and lath boundaries, these precipitates were formed during tempering [13]. Also, the average chemical composition of metallic atoms of Ta-MX particles was measured by EDS analysis (about 100 particles were analyzed, see Table 6) finding that Cr and Fe atoms are dissolved in Ta-MX particles. In addition, many hybrid MX/Z particles (see Table 6) were identified by EDS analysis with the relation  $30 \leq [\text{Fe}] + [\text{Cr}] \leq 40$  at.% [9]. The high frequency of this hybrid particle after tempering suggests that transformation of MX into Z phase has already started [9, 27]. The Figure 5 show a Ta-MX particle with its EDS analysis and diffraction pattern. The indexation of diffraction pattern with a  $[\bar{1}12]$  zone axis (Fig. 5 B) gives a face centered cubic crystal structure consistent with the NaCl-type structure of the MX particles [9, 10]. However, some satellite spots accompanying the principal reflections are also observed in the diffraction pattern (Fig. 5 B) suggesting the existence of compositional modulation associated to the formation of the alternating Cr-rich and Ta-rich layers due to the beginning of the transformation into Z phase [24, 45].





the initial particle size of the Laves phase obtained after tempering (780°C/2 h) increased rapidly from 196 nm to 300 nm at 1440 h of exposure at 650°C which suggests a high growth rate for the particle. Moreover, the growth of the Laves phase does not stop and reaches a value of 400 nm at 8760 h. An explanation to this behavior lies on Laves phase nucleation process. In order to minimize the activation energy barrier for the nucleation, the Laves phase is formed with an orientation relationship to one of the martensitic/ferritic grains. Therefore the nucleus will have a semicoherent, low mobility interface with one adjacent grain and an incoherent mobile interface with another [13, 37]. Next, stable nuclei grow toward the grain with an incoherent interface until reaching its volume fraction and chemical composition of equilibrium [38]. Once the equilibrium is reached, reduction of the interfacial energy of the system starts by the dissolution of small particles and the redeposition of the dissolved species on the surfaces of larger particles (Ostwald ripening) [4]. Theoretically, W has a low diffusion coefficient in the martensitic/ferritic matrix promoting a low coarsening rate. This suggests that rapidly increase in the mean particle size of Laves phase is based on growth stage. Probably, the high W content (3.8%wt) excessively increased the matrix supersaturation, promoting a high growth rate [13, 28]. The table 8 show the calculations of the interface velocity between Laves and  $\alpha$ -ferrite ( $v^{Laves/\alpha}$ ) for the evolution of the mean particle size, according to the registered values in table 7. The interface velocity describes how fast the interface moves during the entire precipitation process and it is an indirect measurement of the growth and coarsening rate [13, 21]. At the initial conditions (T=650°C, t=0) the interface Laves/ $\alpha$  moves into martensitic/ferritic grains with a high rate of  $1 \times 10^{-3}$  nm/s. After 1440h of isothermal aging (650°C) the interface velocity decay two orders of magnitude ( $1.4 \times 10^{-5}$  nm/s) probably due to a reduction of the growth driving force. Afterward, several thousands hours later (8760

h) the interface velocity decreases to  $3.2 \times 10^{-6}$  nm/s. As the Laves/ $\alpha$  interface moves toward the martensitic/ferritic grain consumes W in solid solution since the composition of the matrix reach to the equilibrium value [1,3]. This process reduces the supersaturation of the matrix and consequently the interface velocity of Laves phase particles decreases [13, 46]. Finally, when all the available tungsten is consumed from the matrix during the growth of Laves phase and thus the matrix concentration reaches its equilibrium value, the coarsening stage starts. Probably the interface velocity at the coarsening stage should be even slower, therefore, a slow coarsening rate it is expected for Laves phase [46].

The transformation of Ta-MX into Z phase was investigated by subjecting the chemical composition of particles in extracted replica on the aged samples to EDS-TEM analyses. It was found that Ta-MX, Hybrid MX/Z and Z phase are present in the sample of 1488h with a predominance of Z phase (see Table 6). In contrast, in sample aged for 8760 hours no Ta-MX particles were found and the transformation into Z phase is almost completed; some hybrid particles were observed. For the identification of Z phase by EDS analysis the relation  $[\text{Cr}] + [\text{Fe}] \approx 1.3[\text{Ta}]$  was considered. In addition to this, indexation of diffraction pattern of some particles has been made [25, 26]. Figure 6A shows a zone of the extracted replica of sample aged for 8760 hours which was used for the identification of Z and Laves phase. In general, most of the Ta-MX reaches the chemical composition and tetragonal crystal structure of Z phase. Analysis of diffraction pattern in Fig. 6B confirms a pure tetragonal Z-phase crystal structure with a lattice parameter  $a=0.296\text{nm}$  and  $c=0.739\text{nm}$ , taken from a small Z phase particle probably formed from a previous Ta(C, N) carbonitride [26, 27].

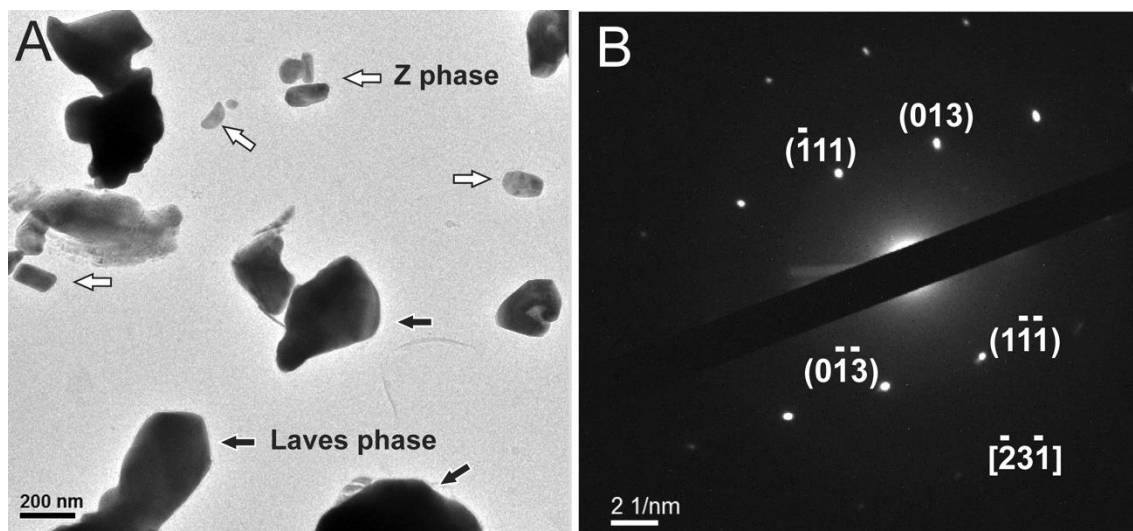


Fig. 6 TEM image of an extracted replica of the alloy after isothermal aging at 650°C after 8760 h. A) Z phase (white arrows) and Laves phase (black arrows). B) Diffraction pattern of CrTa<sub>2</sub>N-Z phase.

On the other hand, in Fig. 7B the diffraction pattern taken from the encircled particle in Fig. 7A shows a tetragonal Z phase crystal structure. The indexation was carried out considering the lattice parameter found by P. Ettmayer,  $a=0.425$  nm and  $c=0.733$  nm. Furthermore, a strong spot (overlapping) of the plane  $(\bar{1}\bar{1}\bar{1})$  can be observed [25-27]. This may be related to a residual trace of the MX cubic structure since some region in the particle is not transformed. In fact, family planes  $\{111\}$  from the TaC/FCC crystal structure have a similar d-spacing compared to family planes  $\{111\}$  of tetragonal structure reported by P. Ettmayer [34], 0.263 nm and 0.278 nm, respectively. This suggests two things; i) particle size of Ta-MX can affect the Z phase transformation [25] and ii) TaC carbides have a kinetics of transformation which is different than Ta(C, N) carbonitrides.

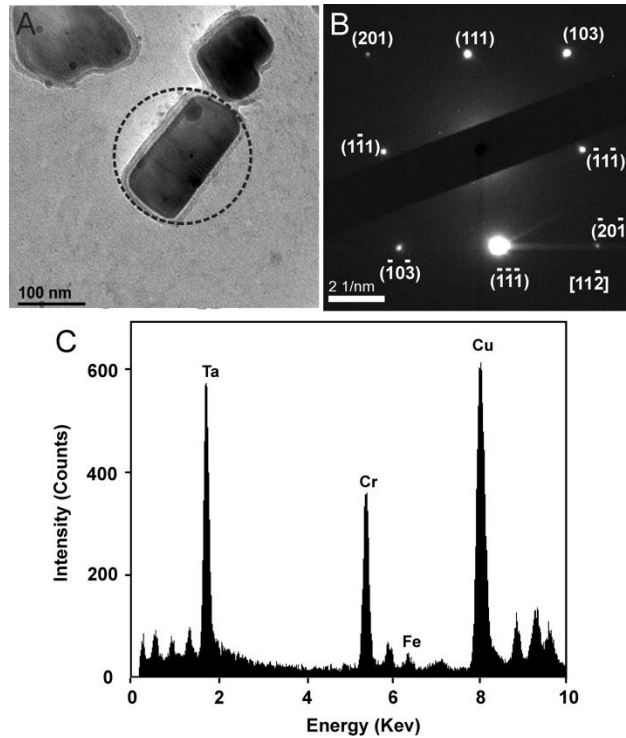


Fig. 7 A) Image of CrTaN-Z phase particle in an extraction replica of the alloy after 8760 h of isothermal aging at 650°C. B) Diffraction pattern of the encircled CrTaN particle in A. C) EDS analysis from particle indicated in A.

As mentioned above it possible that TaC carbides could transform into Z-phase, however its kinetic differs quite from Ta(C, N) and TaN particles. Probably out-diffusion of C control the transformation rate from TaC to Z-phase [47, 48]. This scenario it is suggested from analysis of figure 8, a coarse particle was chemically identified as Z-phase [25, 26]. However, the diffraction pattern of the encircled particle in fig. 8A may not be indexed as tetragonal (see fig. 8B) [25]. Indeed, the particle showed a fcc-like diffraction pattern with a lattice parameter of about 0.45 nm, corresponding to a TaC carbide. Although Cr diffuses into TaC particles, it is probably that remaining C in interstitial sites delay the transition from the NaCl-type crystalline structure (fcc) to a tetragonal system [9, 25]. It is expected

that this behavior is maximized in the center of the particle and then continuously decreases as it is moved towards the particle/matrix interface. Perhaps, the out-diffusion of C atoms is easier near to the surface of the particle, thus N atoms can diffuse into the particle and occupy interstitial sites [19, 27]. Consequently, Cr, C and N gradients inside the particle may create the required condition to generate a core-shell structure between TaC/Z-phase particles [9, 48].

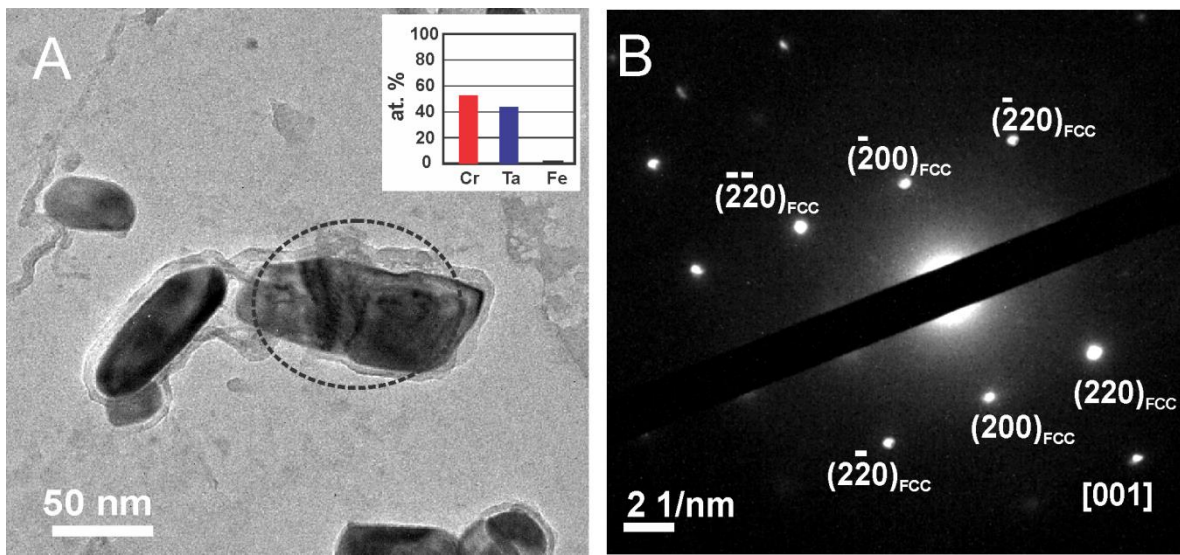


Fig. 8 A) Image of CrTaN-Z phase particle in an extraction replica of the alloy after 8760 h of isothermal aging at 650°C, at the top right is the atomic composition of metallic atoms. B) Diffraction pattern of the encircled CrTaN particle in A.

Furthermore, hybrid particles found at 8760 h suggest that several TaC carbides could not complete the transformation into Z-phase but an Cr enrichment occurs. Also, it is expected that hybrid particles showed a smooth transition from Cr-rich regions, with chemical composition close to Z-phase, towards Cr-poor regions, with compositions close to Ta-rich MX [9, 48]. Finally, analyzed particles with a chemical composition similar to the

described for CrTa<sub>2</sub>N-Z phase have two types of crystalline structure depending of its size and composition of preexistent Ta-MX: i) Tetragonal and ii) NaCl-type crystalline structures. The indexation of diffraction pattern taken from several Z-phase particles as tetragonal confirms the fully transformation of Ta-MX in tetragonal Z phase similar to the CrNbN-Z phase of Austenitic Stainless Steels [25, 41].

### *3.4 Creep test*

The results of the creep tests for the designed alloy (12CrWTaCo) are shown in figure 9. Also, creep data of P91 and P92 steel under similar conditions are input for comparison purposes [13, **Error! Marcador no definido.**]. Creep tests at 650°C show higher creep strength for alloy 12CrWTaCo compared to alloy P91 and P92 steels in the initial stage. However, around 3650 h under creep exposure the rupture occurs with lower creep strength than P91 and P92 steels. Although, a good dispersion of Ta-MX after tempering and high precipitation kinetics of Z phase at 650°C were achieved, a high growth rate of Z phase was observed at 650°C (see Table 7). H. K. Danielsen et al. [49] investigated the interface between the ferrous matrix and nitride precipitates in 12%Cr steels by high resolution transmission electron microscopy finding that TaN and CrTa<sub>2</sub>N are enveloped in an amorphous shell of a few nm thick. This amorphous shell is considered to have a high interfacial energy and it probably promotes a fast precipitation rate and high growth rate of the Z-phase in the designed alloy. On the other hand, the presence of large particle can accelerate the Ostwald ripening mechanism during the coarsening stage when the volume fraction of Z-phase reaches the equilibrium value [21, 43].

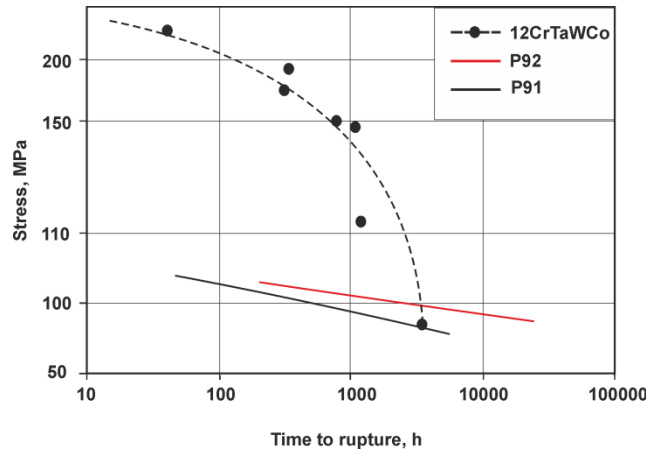


Fig. 9 Tensile creep test showing time to rupture values as a function of applied stress for alloys 12CrTaWCo at 650°C. Creep tests results of P91 and P92 steels under similar conditions are shown as reference data.

Figure 10A and 10B show the growth of Z phase in the aged samples at 650°C for 8760 h. It has been reported that this type of growth is related to the presence of  $\text{Cr}_2\text{N}$  particles [50]. In regards of Laves phase, a similar behavior was observed; although it precipitates with relatively small particle size after tempering (192 nm) at 650°C/8760 h Laves phase reaches a mean radius of 401 nm. Investigation on the growth kinetics of Laves phase in 12%Cr creep resistant steels carried out by O. Prat et al. [51] suggested that Laves phase has an interfacial energy of  $0.6 \text{ J/m}^2$  due to its incoherent interface with the matrix. Furthermore, 3.8%W can also affect the growth driving force, hence higher growth rate is expected for Laves phase. Also, agglomerations of Laves phase in grain and lath boundaries were observed during TEM analysis.



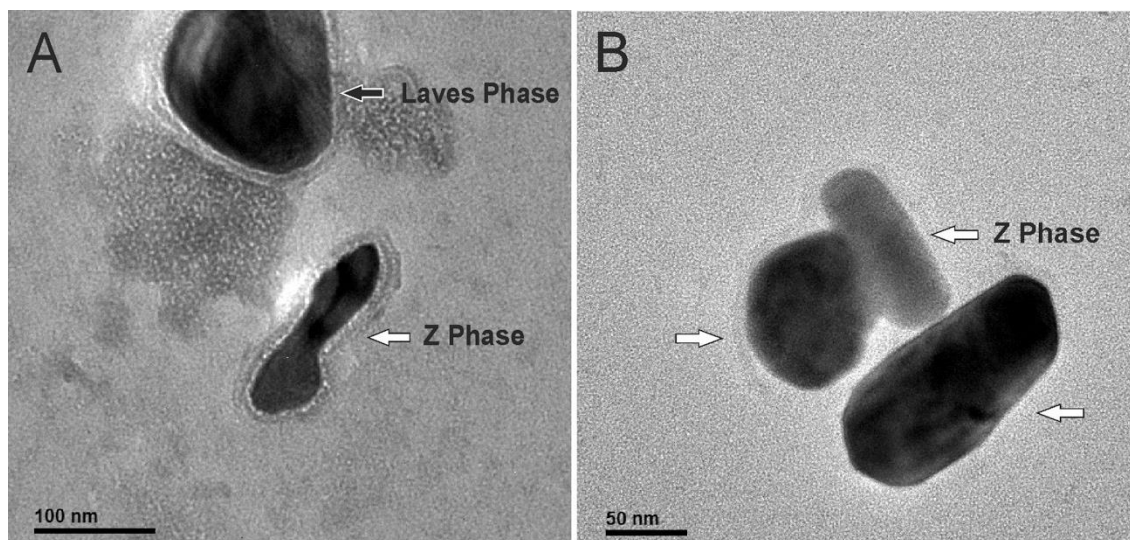


Fig. 10: Growth of Z phase at 8760 h of isothermal aging at 650°C. Image of an extracted replica, A) Z phase (white arrows) and Laves phase (black arrows). B) Z phase (white arrows).

In conclusion, the precipitation of Laves phase after tempering can be reached by the addition of W and Cu while a high kinetics of precipitation of Z phase at 650°C can be achieved by the addition of Ta and avoiding the formation of  $M_{23}C_6$  carbides [13, 26]. However, it was not possible to achieve the same behavior for P91 and P92 steel since Laves and Z phases showed high growth rates. Thus, the degradation of the microstructure during creep exposure at 650°C cannot be avoided due to the loss of the precipitation strengthening caused by the rapid increase of the particle size. In P92 steel the stabilized  $M_{23}(C,B)_6$  carbides and V-MX particles avoid the recovery of subgrain, lath and block structure in the long-term creep due to the slow coarsening rate of these particles associated to lower interface energies [27, 43]. To the authors point of view, the  $M_{23}(C,B)_6$  carbides assure the primary creep strength to the heat resistant steels. Consequently, the  $M_{23}(C,B)_6$  carbides should be included as precipitation hardening particles to ensure long term creep

strength. Finally, further investigations are needed regarding the growth and coarsening stage of Laves and Z phase.

#### **4. Conclusions**

A 12%Cr heat resistant steel was designed and produced to contain Laves phase and Ta-MX as stable phases. Thermodynamic modeling and a microstructural study by transmission electron microscopy were carried out in order to investigate the precipitation of Laves phase. Also, the transformation of Ta-MX into Z phase at 650°C was investigated. The conclusions of this study are summarized as follows:

- The precipitation of Laves phase can be treated as a nucleation process, where by increasing the driving force and the number of available nucleation sites per unit volume the formation of Laves phase at high temperatures can be achieved. Indeed, by adding 3.8%W the stability of Laves Phase rises up to temperatures around 1000°C and 1%Cu increases the available nucleation sites. Indeed, the precipitation of Laves phase after tempering (780°C/2h) was achieved with a mean particle size of 196 nm.
- The identification of Laves phase was carried out by TEM diffraction pattern and EDS-analysis. Diffraction pattern shows a hexagonal close packed crystal structure and the EDS identified the main elements of Laves phase as Fe, Cr and W.
- Measurements of the particle size of Laves phase showed a rapid increment from 196 nm (after tempering 780°C/2h) to 401 nm (isothermal aging 650°C/8740h). This

suggests a fast growth rate for Laves phase due to a high supersaturation and the formation of an incoherent interface with the matrix (highly mobile interface).

- The phase transformation of Ta-MX into Z phase was studied by analyzing the chemical composition of MX particles (only metal atoms were considered) in the alloy after tempering (780°C/2 h) and isothermal aged (1440h and 8760h). Ta-MX and hybrid Ta-MX/Z phase particles were identified confirming that precipitation of Z phase starts during tempering at 780°C/2 h by the formation of hybrid Ta-MX/Z phase particles. No Z phase was found after tempering.
- After isothermal aging at 650°C for 1488 hours, EDS analysis of the  $[\text{Cr}]+[\text{Fe}]/[\text{Ta}]$  ratio of particles confirms the transformation of around 70% of Ta-MX into Z phase. The relation  $[\text{Cr}]+[\text{Fe}]/[\text{Ta}]\approx 1.3$  was considered in order to identify Z phase.
- At 8760 h of isothermal aging at 650°C, Ta-MX particles are fully transformed into Z phase and no Ta-MX particles were found. Analysis of TEM diffraction pattern of particles confirms a tetragonal crystal structure similar to the CrNbN-Z phase in austenitic steels. However, some diffraction pattern taken from coarse Z-phase can be indexed as NaCl-type crystalline structure suggesting that TaC carbides have a different kinetic of transformation. The mean particle size at this stage of Z and Laves phase is 143 nm and 401 nm, respectively.

- A high growth rate is observed for Z phase suggesting that the effect of an amorphous interface is similar to an incoherent interface with the matrix. Also, the presence of large Z phase particles and Cr<sub>2</sub>N may accelerate the growth rate.

## 5. Acknowledgements

The authors would like to thank in particular: “DOCTORADO NACIONAL 21130630” for Doctoral Research Fellowship. Also, project "FONDECYT de Iniciación 11110098", Project "FONDECYT de Iniciación 11121384", "Proyecto de inserción de capital humano avanzado 79112035" and “FONDECYT 1150457” from the Chilean Government, for the financial support of this work. The authors are grateful for the support of the Create-Net project (H2020-MSCA-RISE/644013) for research stays.

## 6. References

- [1] D. Rojas, J. Garcia, O. Prat , G. Sauthoff , A.R. Kaysser-Pyzalla: Mater. Sci. Eng. A, 2011, vol. 528, pp. 5164-5176.
- [2] J. Hald: Int. J. Pres. Ves. Pip., 2008, vol. 85, pp. 30-37.
- [3] A. Aghajani, C. Somsen, G. Eggeler: Acta Mater., 2009, vol. 57, pp. 5093-5106.
- [4] B.S. Srinivas Prasad, V.B. Rajkumar, K.C. Hari Kumar: CALPHAD, 2012, vol. 36, pp. 1–7.
- [5] I. Fedorova, A. Belyakov, P. Kozlov, V. Skorobogatykh , I. Shenkova, R. Kaibyshev: Mater. Sci. Eng. A, 2014, vol. 615, pp. 153–163.
- [6] F. Danoix, R. Danoix, J. Akr, A. Grellier, D. Delagnes: J. Microsc., 2011, Vol. 244, pp. 305-310.
- [7] K. Maruyama, K. Sawada, J. Koike: ISIJ International, 2001, Vol. 41, pp. 641-653.

- [8] K. Rodak, A. Hernas, A. Kielbus: *Mater. Chem. Phys.*, 2003, vol. 81, pp. 483–485.
- [9] L. Cipolla, H. K. Danielsen, D. Venditti, P. E. Di Nunzio, J. Hald, M. A. J. Somers: *Acta Mater.*, 2010, vol. 58, pp. 669–679.
- [10] H. K. Danielsen, J. Hald: *Mater. Sci. Eng. A*, 2009, vol. 505, pp. 169–177.
- [11] F. Abe, M. Taneike, K. Sawada: *Int. J. Pres. Ves. Pip.*, 2007, vol. 84, pp. 3–12.
- [12] U. E. Klotz, C. Solenthaler, P. J. Uggowitzer: *Mater. Sci. Eng. A*, 2008, vol. 476, pp. 186–194.
- [13] D. Rojas, J. Garcia, O. Prat, C. Carrasco, G. Sauthoff, A.R. Kaysser-Pyzalla: *Mater. Sci. Eng. A*, 2010, vol. 527, pp. 3864–3876.
- [14] M. Staubli, K.-H. Mayer, T.-U. Kern, R.W. Vanstone, R. Hanus, J. Stief, K.-H. Schönfeld: in R. Viswanathan, W.T. Bakker, J.D. Parker (Eds.), *Proc. COST 522 - Power Generation into the 21st Century; Advanced Steam Power Plant*, University of Wales and EPRI, 2001, pp. 15-32.
- [15] N. Tanaka, R. Wicks, *Power generation from coal, Measuring and reporting efficiency performance and CO<sub>2</sub> emissions*; International Energy Agency, Paris, France, 2010.
- [16] D. Schmidt, M.C. Galetz, M. Schütze: *Surf. Coat. Tech.*, 2013, vol. 237, pp. 23-29.
- [17] H. K. Danielsen, P. E. DiNunzio, J. Hald: *Metall. Mater. Trans. A*, 2013, vol. 44, pp. 2445-2452.
- [18] M. Taneike, F. Abe, K. Sawada: *Nature*, 2003, vol. 424, pp. 294-296.
- [19] H. K. Danielsen, J. Hald: *CALPHAD*, 2007, vol. 31, pp. 505–514.
- [20] R. Agamennone, W. Blum, C. Gupta, J.K. Chakravartty: *Acta Mater.*, 2009, vol. 54, pp. 3003-3014.
- [21] O. Prat, J. Garcia, D. Rojas, C. Carrasco, A.R. Kaysser-Pyzalla: *Mater. Sci. Eng. A*, 2010, vol. 527, pp. 5976–5983.
- [22] F. Liu, M. Rashidi, L. Johansson, J. Hald, H. O. Andrén: *Scr. Mater.*, 2016, vol. 113, pp. 93–96.
- [23] T. Sakthivel, M. Vasudevan, K. Lahan, P. Parameswaran, K.S. Chandravathi, S. Panneer Selvi, V. Maduraimuthu, M.D. Mathew: *Mater. Sci. Eng. A*, 2014, vol. 591, pp. 111–120.

- [24] M. Yoshizawa, M. Igarashi, K. Moriguchi, A. Iseda, H. G. Armaki, K. Maruyama: Mater. Sci. Eng. A, 2009, vol. 510–511, pp. 162–168.
- [25] H. K. Danielsen, J. Hald, Flemming B. Grumsen, Marcel A.J. Somers: Metall. Mater. Trans. A, 2006, vol. 37, pp. 2633–2640.
- [26] H. K. Danielsen, J. Hald: Scr. Mater., 2009, vol. 60, pp. 811–813.
- [27] H. K. Danielsen, J. Hald, M. A. J. Somers: Scr. Mater., 2012, vol. 66, pp. 261–264.
- [28] O. Prat, J. Garcia, D. Rojas, C. Carrasco, G. Inden: Acta Mater., 2010, vol. 58, pp. 6142–6153.
- [29] TCFE8 - TCS Steels/Fe-Alloys Database, Version 8.0, <http://www.thermocalc.com/products-services/databases/thermodynamic/>. Accessed 21 sept 2016.
- [30] D.R.G. Mitchell, S. Sulaiman: Mater. Charact., 2006, vol. 56, pp. 49–58.
- [31] P. Hofer, H. Cerjak, P. Warbichler: Mater. Sci Technol., 2000, vol. 16, pp. 1221–1225.
- [32] P.J. Goodhew, F.J. Humphreys, Electron Microscopy and Analysis, Taylor and Francis, London, 1988, pp. 39–61.
- [33] K.W. Andrews, D.J. Dyson, S.R. Keown, “Interpretation of Electron Diffraction Patterns”, Adam Hilger Ltd, London, 1971, pp. 71–125 .
- [34] P. Ettmayer: Monatsh. Chem., 1971, vol. 102, pp. 858–863.
- [35] H. K. Danielsen, J. Hald: Energy Mater., 2006, vol. 1, pp. 49–57.
- [36] M.I. Isik, A. Kostka, V.A. Yardley, K.G. Pradeep, M.J. Duarte, P.P. Choi, D. Raabe and G. Eggeler: Acta Mater., 2015, vol. 90, pp. 94–104.
- [37] M.I. Isik, A. Kostka, G. Eggeler: Acta Mater., 2014, vol. 81, pp. 230–240.
- [38] O. Prat, J. García, D. Rojas, J.P. Sanhueza, C. Camurri: Mater. Chem. Phys., 2014, vol. 143, pp. 754–764.
- [39] B. S. Ku and J. Yu: Scr. Mater., 2001, vol. 45, pp. 205–211.
- [40] L. Helis, Y. Toda, T. Hara, H. Miyazaki and F. Abe: Proc. 34th MPA Seminar, Stuttgart, Germany, 2008, MPA Stuttgart, Paper 9.

- [41] H. K. Danielsen: Mater. Sci. Tech., 2016, vol. 32, pp. 126-137.
- [42] M. Tamura, H. Kusuyama, K. Shinozuka, H. Esaka: J. Nucl. Mater., 2007, vol. 367–370, pp. 137–141.
- [43] M. Tamura, K. Shinozuka, K. Masamura, K. Ishizawa, S. Sugimoto: J. Nucl. Mater., 1998, vol. 258-263, pp. 1158-1162.
- [44] M. Tamura , H. Sakasegawa, A. Kohyama, H. Esaka, K. Shinozuka: J. Nucl. Mater., 2004, vol. 329–333, pp. 328–332.
- [45] M. Gao, S. T. Bradley, Y. Cao, D. Jena, Y. Lin, S. A. Ringel, J. Hwang, W. J. Schaff, L. J. Brillson: J. Appl. Phys., 2006, vol. 100, pp. 1-12.
- [46] J.P. Sanhueza, D. Rojas, O. Prat, J. Garcia, R. Espinoza, C. Montalba, M.F. Melendrez: Mater. Chem. Phys., 2017, Vol. 200, pp. 342-353.
- [47] M. Rashidi: Development of a new generation of creep resistant 12% chromium steels: Microstructure of Z-phase strengthened steels, Chalmers University of Technology, Gothenburg, Sweden, 2017, pp. 48-51.
- [48] M. Rashidi, H. O. Andrén, F. Liu: Microsc. Microanal., 2017, Vol. 23, pp. 360-365.
- [49] H.K. Danielsen, S. Kadkhodazadeh, F.B. Grumsen, M.A.J. Somers: Philos. Mag., 2014, vol. 94, pp. 2339–2349.
- [50] M. Y. Kima, S. M. Hong, K. H. Lee, W. S. Jung, Y. S. Lee, Y. K. Lee, J. H. Shim: Mater. Charact., 2017, vol. 129, pp. 40–45.

## Tables

Table 1: Chemical composition of the 12CrWTaCo alloy (wt%).

| Fe      | Cr   | Mn  | Ta   | W   | Cu  | C    | B     | N    | Si  | Co  |
|---------|------|-----|------|-----|-----|------|-------|------|-----|-----|
| Balance | 12.9 | 0.6 | 0.85 | 3.8 | 1.0 | 0.06 | 0.001 | 0.05 | 0.5 | 4.2 |

Table 2: Lattice parameters considerer for TaC, Ta(C,N), TaN, Z and Laves phase.

| Phase   | Crystal structure | a (nm) | c (nm) |
|---------|-------------------|--------|--------|
| TaC     | FCC               | 0.455  | -      |
| Ta(C,N) | FCC               | 0.437  | -      |
| TaN     | FCC               | 0.434  |        |

|                |                                 |       |       |
|----------------|---------------------------------|-------|-------|
| CrTa-N-Z phase | Tetragonal (Danielsen and Hald) | 0.296 | 0.739 |
|                | Tetragonal (Ettmayer)           | 0.425 | 0.733 |
| Laves phase    | HCP                             | 0.474 | 0.673 |

Table 3: Chemical composition (at.%) of the equilibrium phases at Austenization temperature (1070°C).

| Phase     | Fe    | Cr    | Co   | W     | Si   | Mn   | Cu  | Ta    | C     | N     |
|-----------|-------|-------|------|-------|------|------|-----|-------|-------|-------|
| Austenite | 77.79 | 14.17 | 4.07 | 1.18  | 1.02 | 0.62 | 0.9 | 0.018 | 0.171 | 0.062 |
| Ta-MX     | -     | 2.52  | -    | 0.076 | -    | -    | -   | 47.75 | 41.33 | 8.32  |

Table 4: Chemical composition (at.%) of the equilibrium phases at tempering temperature (780°C).

| Phase                          | Fe    | Cr    | Co    | W     | Si    | Mn   | Cu    | Ta    | C     | N    |
|--------------------------------|-------|-------|-------|-------|-------|------|-------|-------|-------|------|
| Ferrite                        | 79.47 | 13.76 | 4.22  | 0.28  | 1.05  | 0.63 | 0.59  | -     | -     | -    |
| Laves                          | 42.53 | 12.48 | 0.44  | 32.87 | 0.125 | 0.22 | 1.13  | 0.015 | -     | -    |
| M <sub>23</sub> C <sub>6</sub> | 15.81 | 57.22 | 0.059 | 5.15  | -     | 1.07 | -     | -     | 20.69 | -    |
| Ta-MX                          | -     | 1.48  | -     | 0.038 | -     | -    | -     | 47.36 | 47.43 | 2.54 |
| Cu-rich                        | 0.53  | 0.19  | 0.028 | 2.04  | -     | 0.88 | 96.50 | -     | -     | -    |

Table 5: Chemical composition (at.%) of the equilibrium phases at creep test and isothermal aging temperature (650°C).

| Phase                          | Fe    | Cr    | Co    | W     | Si   | Mn   | Cu    | Ta    | C     | N    |
|--------------------------------|-------|-------|-------|-------|------|------|-------|-------|-------|------|
| Ferrite                        | 79.94 | 13.69 | 4.25  | 0.14  | 0.16 | 0.62 | 0.30  | -     | -     | -    |
| Laves                          | 42.40 | 14.16 | 0.28  | 32.95 | 0.16 | 0.27 | 9.78  | 0.032 | -     | -    |
| M <sub>23</sub> C <sub>6</sub> | 11.45 | 62.3  | 0.02  | 3.75  | -    | 1.83 | -     | -     | 20.69 | -    |
| Ta-MX                          | -     | 2.086 | -     | 0.013 | -    | -    | -     | 47.94 | 48.41 | 1.55 |
| Cu-rich                        | 0.29  | -     | 0.013 | 1.53  | -    | 1.08 | 97.00 | -     | -     | -    |

Table 6: Average composition of Laves phase, Ta-MX and Z phase in the alloy after tempering and isothermal aging. The chemical composition was measured by EDS analysis and only metal atoms were considered.



| Sample       | Particles Measured | Particle Type  | Frequency | Average chemical composition (at. %) |    |    |    |
|--------------|--------------------|----------------|-----------|--------------------------------------|----|----|----|
|              |                    |                |           | Cr                                   | Ta | Fe | W  |
| As-Treated   | 100                | TaC or Ta(C,N) | 58        | 15                                   | 78 | 7  | -  |
|              |                    | Hybrid MX/Z    | 42        | 31                                   | 61 | 8  | -  |
|              |                    | Z phase        | Not found | -                                    | -  | -  | -  |
|              | 40                 | Laves          | 100       | 16                                   | -  | 46 | 38 |
| 650°C 1488 h | 100                | TaC or Ta(C,N) | 13        | 12                                   | 82 | 4  | -  |
|              |                    | Hybrid MX/Z    | 17        | 29                                   | 63 | 7  | -  |
|              |                    | Z phase        | 70        | 55                                   | 37 | 8  | -  |
|              | 40                 | Laves          | 100       | 15                                   | -  | 47 | 38 |
| 650°C 8760 h | 100                | TaC or Ta(C,N) | Not found | -                                    | -  | -  | -  |
|              |                    | Hybrid MX/Z    | 7         | 36                                   | 58 | 6  | -  |
|              |                    | Z phase        | 93        | 54                                   | 41 | 5  | -  |
|              | 40                 | Laves          | 100       | 16                                   | -  | 48 | 37 |

Table 7: Average particle size of precipitates after isothermal aging at 650°C (time in hours and size in nanometers), error =  $d \pm k_1 \times S$  where  $k_1 = 1.96/\sqrt{n}$  and n is the number of measured precipitates.

| Phase    | 0 h          | 1488 h       | 8760 h       |
|----------|--------------|--------------|--------------|
| Ta(C, N) | $30 \pm 2$   | -            | -            |
| TaC      | $137 \pm 15$ | $138 \pm 15$ | -            |
| Laves    | $196 \pm 35$ | $300 \pm 34$ | $401 \pm 41$ |
| Z        | -            | $80 \pm 15$  | $143 \pm 15$ |

Table 8: Interface velocity of Laves phase during its precipitation at 650°C in the alloy 12CrWTaCo. The calculi were carried out with the formula ( $v^{Laves/\alpha} = \frac{x}{2t}$ ) where “x” is the mean radius of the particle at the time “t”. The interface velocity at t=0 was calculated by the set conditions during tempering (780°C/2h).

| Time (h) | Interface velocity (nm/s) |
|----------|---------------------------|
| 0        | $1.0 \times 10^{-3}$      |
| 1440     | $1.4 \times 10^{-5}$      |
| 8760     | $3.2 \times 10^{-6}$      |